Chapter 2

Trialkoxysilane-functionalized monometallic, bimetallic, and trimetallic noble metal nanoparticles mediated non-enzymatic sensing of glucose by resonance Rayleigh scattering

2.1. Introduction

Noble metal nanoparticles with surface functionalization by a functional trialkoxysilane (e.g., 3-aminopropyltrimethoxysilane (3-APTMS) and 3-glycidoxypropylytrimethoxysilane (3-GPTMS)) have potential use in catalytic applications. (Pandey and Chauhan, 2012; Pandey et al.,2014a; Pandey et al., 2014b; Pandey et al., 2014c; Pandey et al., 2014d; Pandey et al., 2014e; Pandey et al., 2015; Pandey et al., 2016b; Pandey et al.,2016c). Previous work has demonstrated their use for synthesizing noble metal nanoparticles using 3-APTMS and 3-GPTMS. It has been reported that 3-APTMS capped gold ions are converted into nanoparticles in the presence of reducing agents such as 3-GPTMS, cyclohexanone, tetrahydrofuran hydroperoxide, and formaldehyde. The controlled conversion of gold cations to gold nanoparticles within one minute was enabled by the reducing functionality of 3-APTMS, 3-GPTMS, cyclohexanone, and formaldehyde (Pandey et al., 2018; Pandey et al., 2016d; Pandey et al., 2021a; Pandey et al., 2020; Pandey et al., 2021b;). We demonstrated that 3-APTMS in the presence of cyclohexanone allows for the conversion of potassium ferricyanide to Prussian blue; these studies showed the reducing capability of cyclohexanone in the presence of 3-APTMS to convert Fe^{+3} to Fe^{+2} (Pandey et al., 2005; Pandey et al., 2016a; Pandey et al., 2015). Uppal et al, found that cyclohexanone enables gold cations to be converted into nanoparticles (Uppal, et al., 2013). We have demonstrated that AuNPs that were prepared with cyclohexanone undergo rapid agglomeration, which can be controlled by the presence of 3-APTMS; this method allows gold or palladium cations to be converted into nanoparticles. The micellar behaviour of 3-APTMS enables the conversion of hydrophilic cations to stable AuNPs in the presence of hydrophobic cyclohexanone; this method is appropriate for many applications. These studies indicate that functional trialkoxysilanes can function as reducing

and stabilizing agents for the controlled conversion of noble metal cations into nanoparticles. A similar process efficiently enables the controlled synthesis of other noble metal nanoparticles such as silver nanoparticles and palladium nanoparticles. Synergistic interactions associated with bimetallic and trimetallic nanoparticles were shown to be associated with dramatic changes in catalytic performance. The functional trialkoxysilane reducing agent can be used for the processing of monometallic, bimetallic, and trimetallic nanoparticles. Functional trialkoxysilane functionalized bimetallic Ag-Au, Au-Ag, Au-Pd, and Pd-Au nanoparticles were shown to exhibit catalytic ability for many applications. It has been shown that gold nanoparticles can be prepared using a wide range of functional trialkoxysilane concentrations; this approach may be used to control the resonance Rayleigh scattering (RRS) intensity and enable enzyme-free catalysis of the analyte (El Kurdi and Patra, 2018; Samokhvalov et al., 2020; Pandey et al., 2012). This method is straightforward, stable, and selective; it offers an excellent linear dynamic range under physiological conditions, particularly for glucose sensing. The synchronous fluorescence signal recorded from functional trialkoxysilane-functionalized gold nanoparticles was found to be linearly dependent on the concentration of glucose. Accordingly, a study was undertaken to understand the functional trialkoxysilane -functionalized monometallic, bimetallic, and tri-metallic noble metal nanoparticle-mediated sensing of glucose by synchronous fluorescence spectroscopy (SFS). As-made noble metal nanoparticles, bimetallic nanoparticles, and trimetallic nanoparticles are based on SFS; these novel findings are described for the first time in this study.

2.2. Experimental section

2.2.1. Materials and reagent

Formaldehyde, ethylene glycol, polyvinylpyrrolidone (PVP), methanol, 3-glycidoxyporpyltrimethoxysilane (3-GPTMS), sodium borohydride (NaBH4), 3-aminopropyletrimethoxysilane (3-APTMS), and trachloropalladate (K2PdCl4) were purchased from Sigma Aldrich Chemicals Pvt Ltd (Bangalore, India). Methanol, silver nitrate (AgNO3), tetrachloroauric acid (HAuCl4) and glucose were purchased from Himedia Laboratories (Mumbai, India). Phosphate buffer solution and double-distilled water were used in the experiments.

2.2.2. Microwave-assisted synthesis of trialkoxysilane functionalized noble metal nanoparticles and their multimetallic analogues

2.2.2.1. Microwave-assisted 3-APTMS and 3-GPTMS mediated controlled synthesis of gold nanoparticles

60 μL of an methanolic solution of HAuCl4 (0.050 M) was prepared.150 μL of an ethylene glycolic solution of 3-APTMS (0.05 M) was added to HAuCl4 solution. The reaction mixture was stirred on a cyclo vertex mixture for 1 min, followed by the addition of 3-glycidoxypropyletrimethoxysilane (0.5 M in ethylene glycol). The mixture was then incubated in a microwave oven for 10 s. The incubation process was repeated 1-4 times, resulting in the formation of dark red-colored AuNPs. The as-made nanoparticles were characterized using transmission electron microscopy.

2.2.2.2. Microwave-assisted 3-APTMS and 3-GPTMS mediated synthesis of silver nanoparticles

180 μL of a methanolic solution of $AgNO_3$ (0.025 M) was prepared. 45 μL of 3-APTMS (0.5 M) in ethylene glycol solution was added in the $AgNO_3$ solution. The reaction mixture was stirred on a cyclo vertex mixture for 2 min, followed by the addition of 3-glycidoxypropyletrimethoxysilane (3M in ethylene glycol). The mixture was then incubated in a microwave oven for 20 s. The incubation process was repeated 3-5 times, resulting in the formation of dark, yellow-coloured silver nanoparticle sols. The as-made nanoparticles were characterized using transmission electron microscopy.

2.2.2.3. Microwave-assisted 3-APTMS and formaldehyde mediated controlled synthesis of palladium nanoparticles

A 100 μL solution of K_2PdCl_4 (0.020M) in ethylene glycol was mixed with 3-APTMS (0.5 M) in ethylene glycol, followed by the addition of 100 μL of HCHO under stirring. The reaction mixture was incubated in a microwave oven for 10 seconds. The incubation process was repeated 3-7 times, resulting in the formation of dark, black-coloured palladium nanoparticle sols. The as-made nanoparticles were characterized using transmission electron microscopy.

2.2.2.4. Microwave-assisted 3-APTMS and 3-GPTMS mediated controlled synthesis of Au-Ag bimetallic nanoparticles

A 240 μL methanolic solution of $AgNO_3$ (0.025 M) was mixed with 60 μL solution of 3-APTMS (0.5 M) in ethylene glycol, followed by the addition of 160 μL of the gold nanoparticle sol and stirring. A 60 μL solution of 3-GPTMS (3 M) in ethylene glycol was added into the reaction mixture, followed by incubation in a microwave oven for 10 s. The incubation process

was repeated 3-7 times, resulting in the formation of dark yellowish-orange color bimetallic (Au-Ag) sols. The as-made nanoparticles were characterized using transmission electron microscopy.

2.2.2.5. Microwave-assisted 3-APTMS, 3-GPTMS, and formaldehyde mediated controlled synthesis of Ag -Pd bimetallic nanoparticles

200 μL of K_2PdCl_4 (0.025 M in ethylene glycol) was mixed under stirring conditions; 200 μL of previously-synthesized silver nanoparticle colloidal suspension (made as discussed in section 2.2.2.2) was added as described earlier. 180 μL of formaldehyde was added to the stirring mixture. This mixture was incubated for 6 s in a microwave oven. This step was repeated 5-12 times in order to create a dark yellowish-orange colored colloidal suspension of bimetallic Ag-Pd nanoparticles.

2.2.2.6. Microwave-assisted 3-APTMS, 3-GPTMS, and formaldehyde mediated controlled synthesis of Au-Ag-Pd trimetallic nanoparticles

A 100 μL solution of K_2PdCl_4 (0.025M) in ethylene glycol was prepared; 25 μL solution of 3-APTMS (0.5 M) in ethylene glycol was added to this solution. 200 μL of previously-synthesized Au-Ag bimetallic nanoparticle colloidal suspension (made as discussed in section 2.2.2.4) was added as mentioned earlier, followed by the addition of 100 μL of HCHO to the reaction mixture, which was allowed to incubate in a microwave oven for 20 seconds. The incubation process was repeated for 2-5 times, resulting in the formation of dark yellowish-orange colored trimetallic Au-Ag -Pd sols. The as-made nanoparticles were characterized using transmission electron microscopy.

2.2.2.7. Microwave-assisted 3-APTMS, 3-GPTMS, and formaldehyde mediated controlled synthesis of Au-Pd bimetallic nanoparticles

A 200 µL K_2PdCl_4 (0.025 M in ethylene glycol) was mixed under stirring. 200 µL of previously-synthesized gold nanoparticle colloidal suspension (made as discussed in section 2.2.2.1) was added as mentioned earlier. 150 µL of formaldehyde was added to the stirring mixture. The mixture was incubated for 6 s in a microwave oven. This step was repeated 4-10 times in order to create a dark yellowish-orange colored colloidal suspension of bimetallic Au-Pd nanoparticles. The synthesis of gold and palladium bimetallic nanoparticles with Au:Pd ratios of 20:80 and 80:20 was performed using a similar procedure.

2.2.3. Instrumentation

X-ray diffraction (XRD) data were collected with a Miniflex II diffractometer (Rigaku, Tokyo, Japan). Transmission electron microscopy (TEM) was performed using a JEM-2100F electron microscope (JEOL, Tokyo, Japan). UV-Vis spectra were recorded by Hitachi F2900 specrtophotometer. An F7000 fluorescence spectrophotometer (Hitachi, Tokyo, Japan) was used to obtain SFS data. The wavelength interval was maintained at 0 nm ($\Delta\lambda= 0$ nm) to obtain the resonance Rayleigh scattering spectra.

2. 3. Results and discussion

2. 3.1. Functional trialkoxysilane mediated synthesis of AuNP, AgNP, and PdNP and their multimetallic analogues

3-APTMS capped noble metal cations may be converted into monometallic, bimetallic, and trimetallic nanoparticles in the presence of a small organic reducing agent (e.g.,

cyclohexanone, tetrahydrofuran hydroperoxide, or formaldehyde) or 3-GPTMS. These as-made nanoparticles can be made insensitive to pH changes.
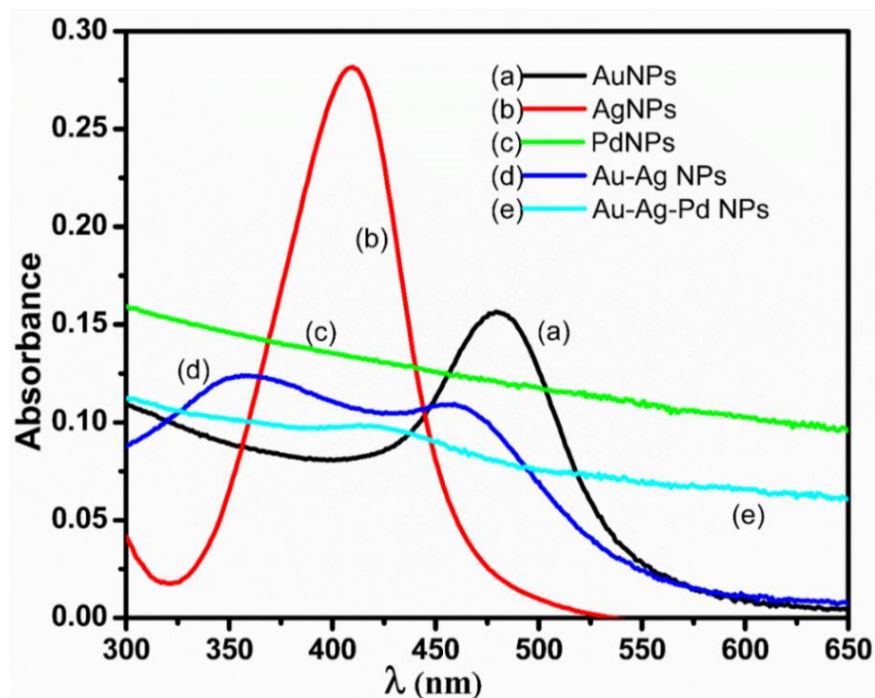

Fig. 2.1. UV–Vis spectra of the nanoparticles (a)gold nanoparticles (b) silver nanoparticles (c) palladium nanoparticles (d) bimetallic (Au–Ag) nanoparticles (e) trimetallic (Au–Ag–Pd) nanoparticles.
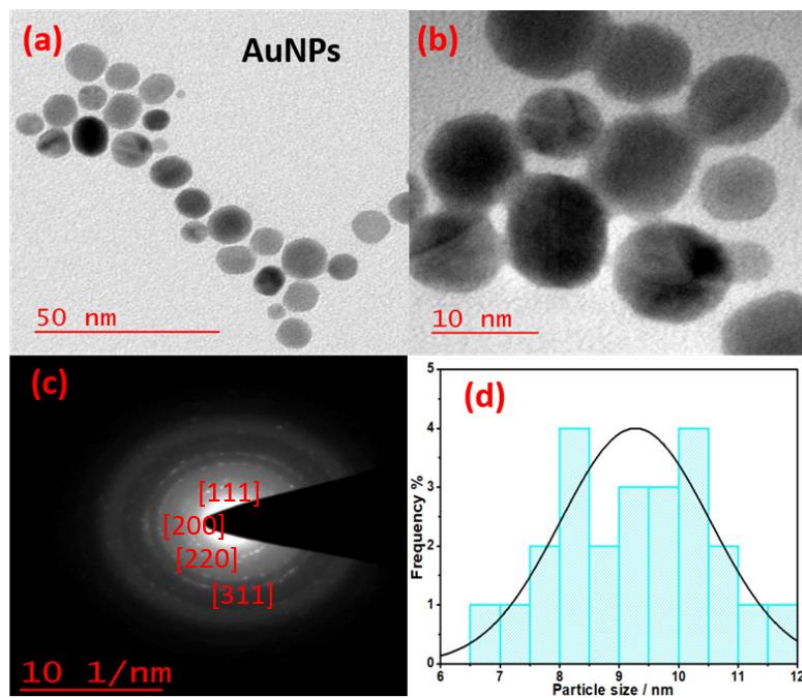
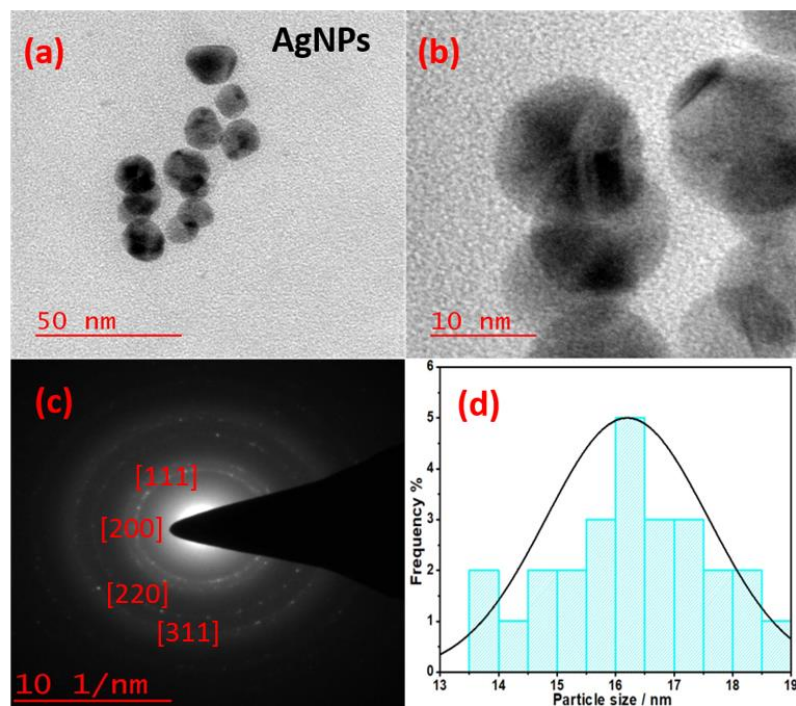Fig. 2.2. (a) & (b) TEM images (c) SAED pattern and (d) particle size distribution graph of gold nanoparticles.

Fig. 2.3. (a) & (b) TEM images (c) SAED pattern and (d) particle size distribution graph of silver nanoparticles.
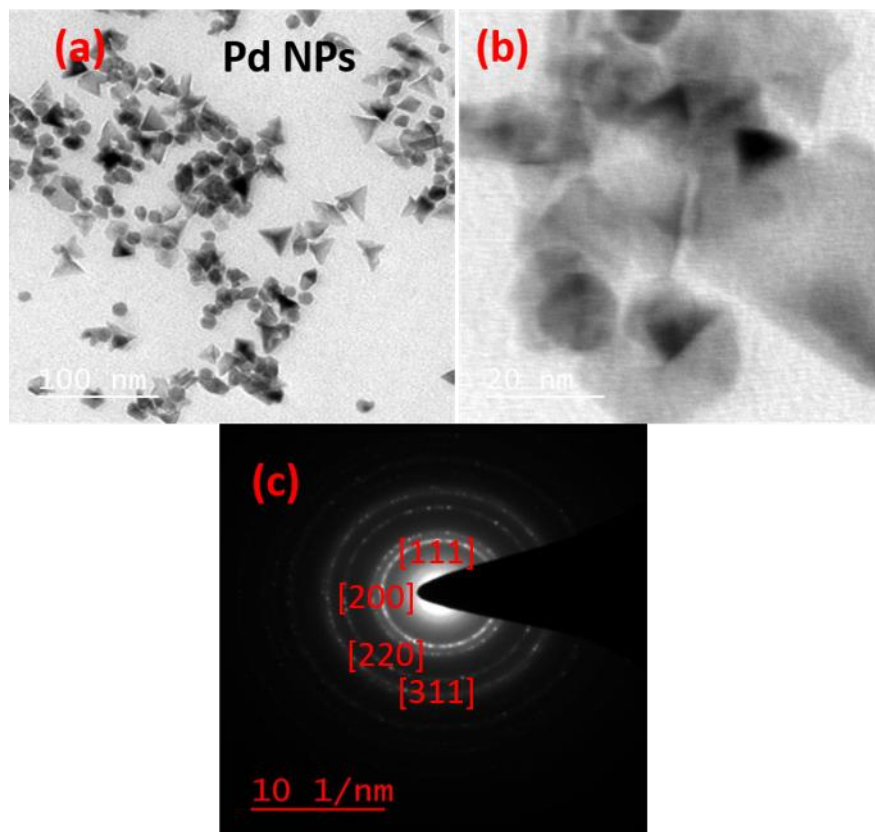
Fig. 2.4. (a) & (b) TEM images (c) SAED pattern of palladium nanoparticles.

The functional groups attached to the trialkoxysilanes are microwave active during microwave incubation. Metal cations can be easily converted into nanoparticles by this method. It is noteworthy that microwave processing enables the rapid synthesis of bimetallic nanoparticles and trimetallic nanoparticles with sufficient stability for practical applications. The UV–Vis spectra shown in Fig. 2.1 confirm the specific SPR of gold, silver, palladium, Au–Ag, and Au–Ag–Pd nanoparticles. Fig. 2.1 line (a) for gold nanoparticles shows an absorption maxima at around 495 nm, and Fig. 2.1 line (b) for silver nanoparticles shows an absorbance at around 406 nm. The palladium nanoparticles do not show characteristic absorption in the visible region as shown in line (c) (Fig. 2.1). The absorption is close to 360 nm for silver and 461 nm for gold for their corresponding gold–silver bimetallic nanoparticles

as shown in line (d) (Fig. 2.1). Fig. 2.1 line (e) shows the absorption spectrum for the Au–Ag–Pd trimetallic nanoparticles. The synthesized nanoparticles were further confirmed by TEM and EDX analysis. TEM images of the monometallic, bimetallic, and trimetallic nanoparticles

TEM images of monometallic and their multimetallic anologue nanoparticles that were obtained from the functional trialkoxysilane -mediated conversion of the metal cations. These nanoparticle TEM images were shown in (Fig.2.2-Fig.2.8). Fig. 2.2a and b, depict the TEM images that were recorded at different magnifications of gold nanoparticles, and Fig. 2.2c and d show the SAED pattern and particle size distribution graph of gold nanoparticles. The average particle size was found to be 9-10 nm. Likewise, Fig. 2.3a, b and Fig. 2.4a, b show the TEM images of silver and palladium nanoparticles were recorded at different magnifications, and the SAED pattern and particle size distribution of silver nanoparticles were shown in Fig. 2.3c and Fig. 2.3d, respectively. The average particle size of silver nanoparticles was found to be 16-17 nm. Fig. 2.4c shows the SAED pattern of palladium nanoparticles and the average particle size was found to be 4 nm. The TEM images of bimetallic nanoparticles in Fig. 2.5a, b and Fig. 2.6a, b show the TEM images of Au-Ag and Ag-Pd bimetallic nanoparticles were recorded at different magnifications, respectively, and the SAED pattern and particle size distribution of Au-Ag and Ag-Pd bimetallic nanoparticles are shown in Fig. 2.5c, d and Fig.2.6c, d, respectively. The average particle size of Au-Ag and Au-Pd bimetallic nanoparticles was 22 nm and 13 nm, respectively. Bimetallic (Au-Pd) nanoparticles made at two different metal ratios (Au/Pd 80:20 and 20:80). Fig. 2.7a and b show the TEM images recorded at different magnifications of the Au-Pd bimetallic nanoparticles at a metal ratio of 80:20. The SAED pattern and particle size of the Au-Pd bimetallic nanoparticles were shown

in Fig. 2.7c and d, respectively. The average particle size of Au-Pd bimetallic nanoparticles was found to be 12 nm.

Fig. 2.8a and b show TEM images of the Au-Ag-Pd trimetallic nanoparticles. The SAED pattern and EDX of the Au-Ag-Pd trimetallic nanoparticle were shown in Fig. 2.8c and Fig. 2.8d respectively. TEM images of the monometallic, bimetallic, and trimetallic nanoparticles that were obtained from the functional trialkoxysilane-mediated controlled conversion of the metal cations. These findings confirm that the functional trialkoxysilane efficiently allows the controlled reduction of noble metal cations into nanoparticles in a variety of configurations to yield noble metal nanoparticles and multimetallic nanoparticles.
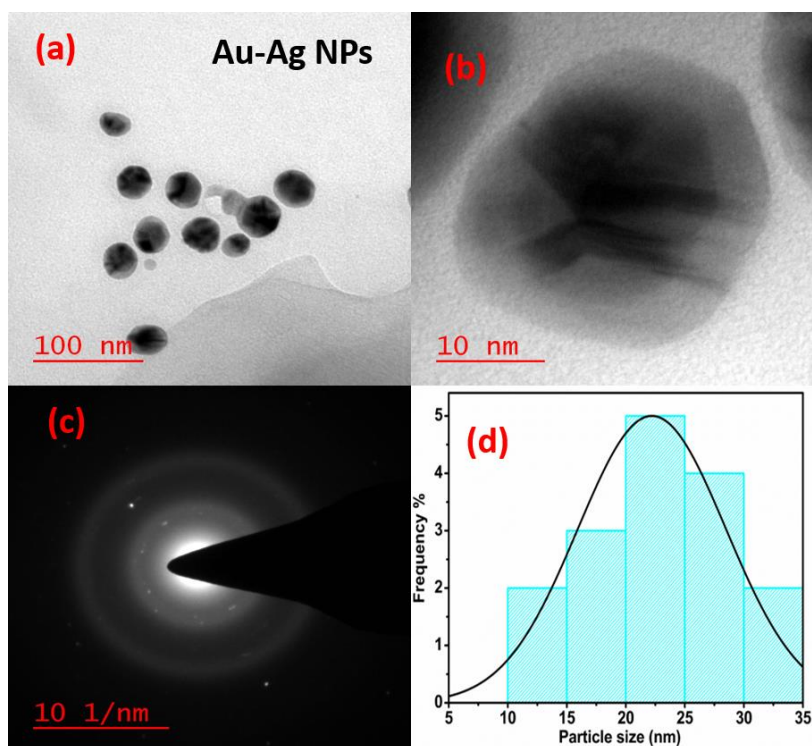

Fig. 2. 5. (a) & (b) TEM images (c) SAED pattern and (d) particle size distribution graph of Au-Ag bimetallic nanoparticles.
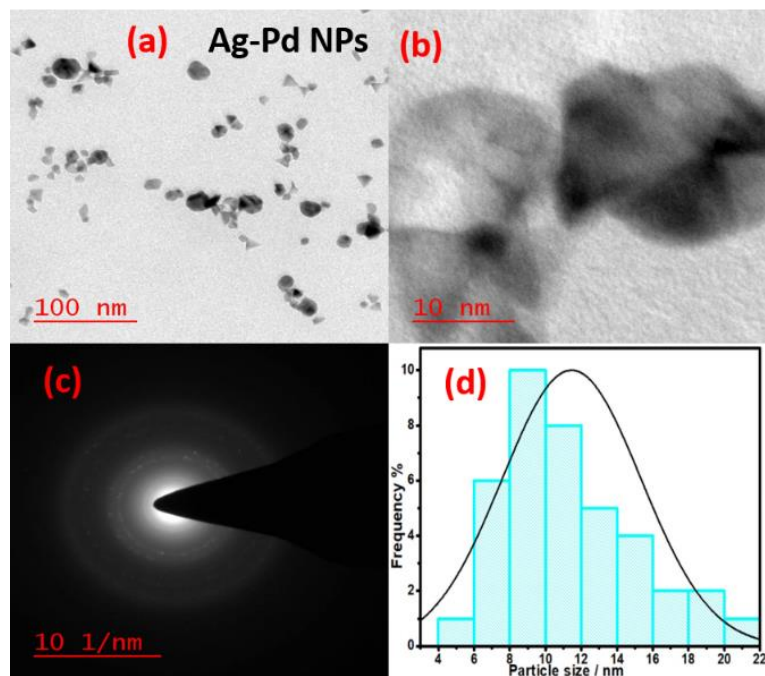
Fig. 2.6. (a) & (b) TEM images (c) SAED pattern and (d) particle size distribution graph of Ag-Pd bimetallic nanoparticles.
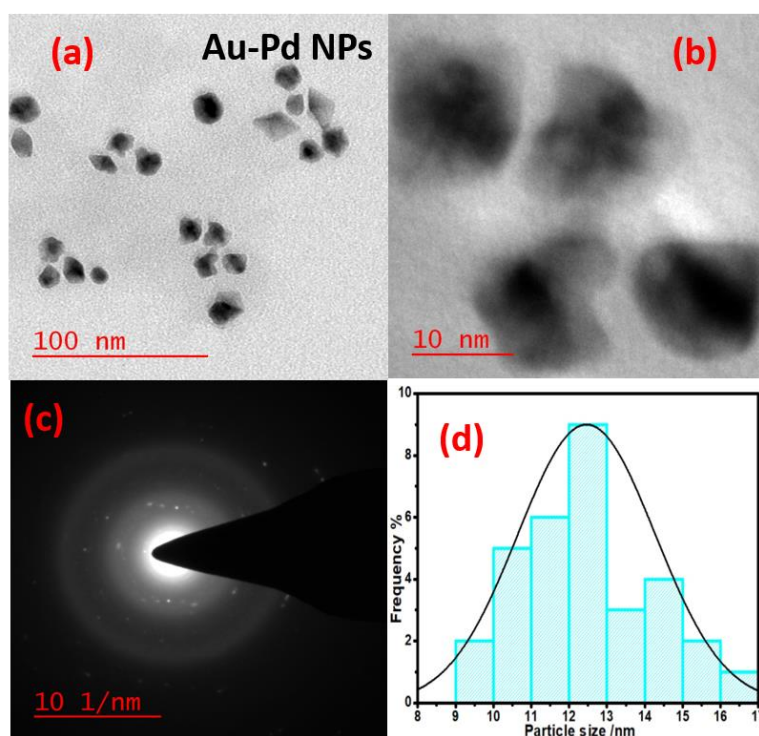

Fig. 2.7. (a) & (b) TEM images (c) SAED pattern and (d) particle size distribution graph of Au-Pd bimetallic nanoparticles.
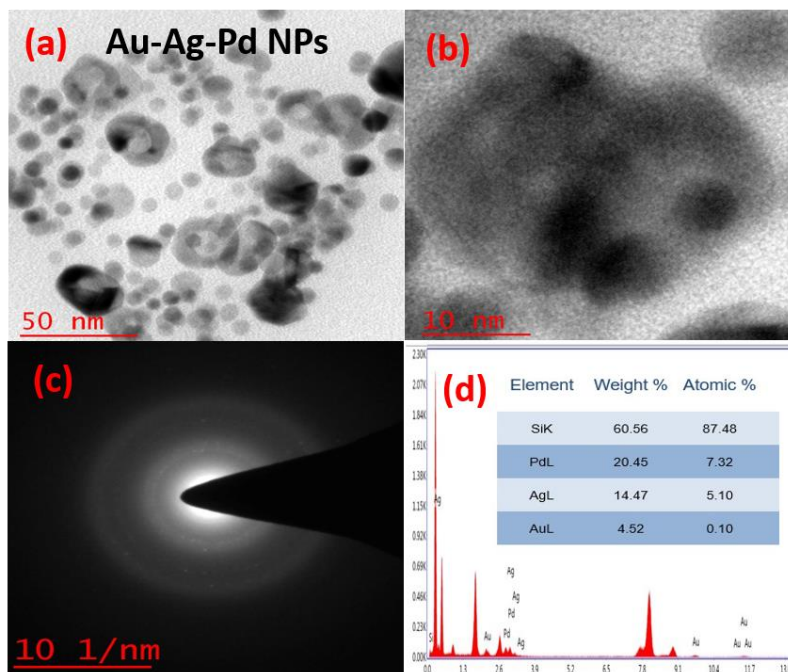
Fig. 2.8. (a) & (b) TEM images (c) SAED pattern and (d) particle size distribution graph of Au-Ag-Pd trimetallic nanoparticles.

These nanoparticles have been further characterized by XRD analysis. Fig. 2.9 shows the XRD analysis of PdNPs (Fig.2.9a), AgNPs (Fig.2.9b), and AuNP (Fig. 2.9c) nanoparticles, respectively. Silver and gold have very similar lattice parameters and appear to merge. In addition, the formation of bimetallic and trimetallic nanoparticles is indicated by the XRD pattern of these nanoparticles, which deviates slightly from their individual 2Ө angles. The XRD analysis of bimetallic (Au-Ag, Au-Pd, Ag-Pd) and trimetallic (Au-Ag-Pd) nanoparticles are shown in Fig. 2.10 (a-d). Trimetallic nanoparticles (planes for Au-Ag at angles of 38.1[111], 44.4[200], 77.5[311] and for the Pd at angles of 39.7[111], 46.4[200]), Likewise, the planes of Ag-Pd bimetallic nanoparticles are (at an angle of 44.4(200) and 40.2[111], 46.5[200], 67.9 [220], 81.8[311] planes correspond to Ag and Pd metal), similarly, planes for

Au-Pd bimetallic nanoparticles (at an angle of 38.1[111], 44.3[200], 64.5[220], 77.5[311] and

40.0[111], 46.5[200], 68.1 [220], and 81.8[311] planes correspond to Au and Pd metal).The

corresponding planes as evaluated from diffraction patterns confirm the role of the

trialkoxysilane in the controlled processing of noble metal nanoparticles and multimetallic
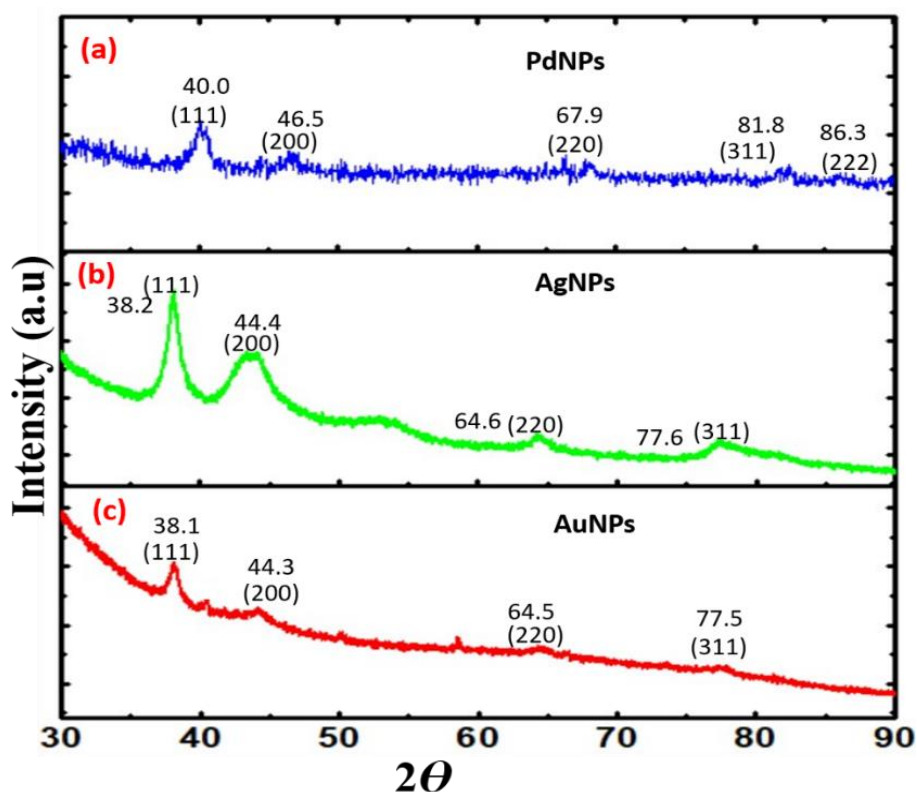
nanoparticles.

Fig. 2.9**.** XRD profile of XRD profile of (a) PdNPs, (**b**) AgNPs, (c) AuNPs.

The formation of monometallic, bimetallic and trimetallic noble metal nanoparticles can

further be evaluated from the results shown in Fig.2.1 based on UV-VIS spectroscopy

justifying the existence of bimetallic and trimetallic configurations as individual absorption

peak for monometallic nanoparticles is shifted in Au-Ag and Pd-Au-Ag. Further [Pandey et al

2015] has already demonstrated the formation of Au-Pd and Ag-Pd following either

simultaneous or sequential mode on more than one noble metal cation's reduction. The XRD observation as shown in 2.10 revealed the presence of two or more than two sets of individual diffraction pattern revealing the existence of mixture or heterogeneous nanoparticles however the UV-VIS spectra (Fig.2.1) does not support the same and require further detailed investigation based on HRTEM imaging along with controlling the ratio of monomeric constituent in bimetallic and trimetallic configurations followed by determining their lattice constant which constitutes future projection of current thesis work
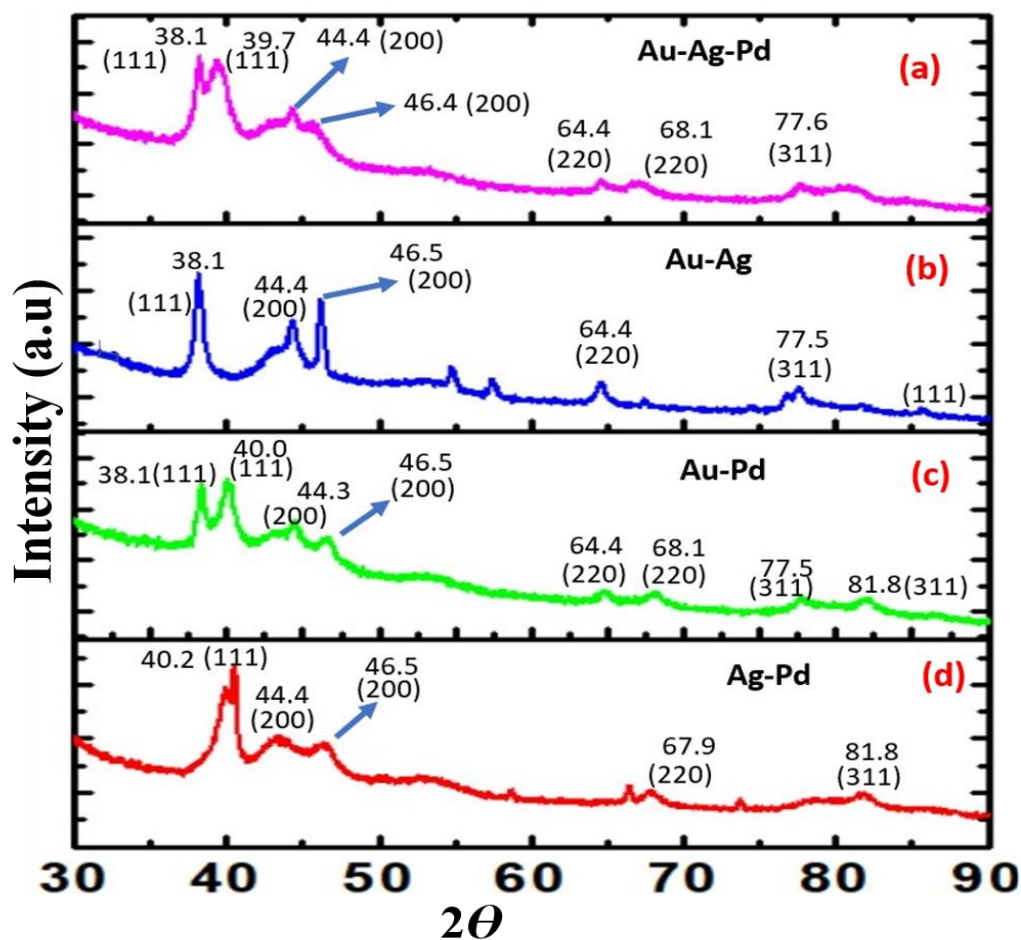

Fig. 2.10. XRD profile of **(a)** trimetallic (Au-Ag-Pd) NPs, **(b)** bimetallic (Au-Ag) NPs, **(c)** bimetallic (Au-Pd) NPs, and **(d)** bimetallic (Ag-Pd) NPs.

2. 3.2. Synchronous fluorescence spectroscopy of functional trialkoxysilane - functionalized noble metal nanoparticles and multimetallic nanoparticles for non-enzymatic sensing of glucose

Synchronous fluorescence spectroscopy has been extensively utilized to detect compounds in solution. Previous studies have demonstrated the detection of blood glucose using gold nanoparticles. These efforts led us to investigate the role of as-made metal nanoparticles, bimetallic nanoparticles, and trimetallic nanoparticles in enzyme-free glucose sensing. Since bimetallic and trimetallic nanoparticles may be using different ratios of noble metal cations with the functional trialkoxysilane, we investigated the performance of as made AuNPs, AgNPs, PdNPs, Ag-Au NPs, Ag-Pd NPs, Au-Pd NPs, and Ag-Au-Pd NPs for enzyme-free sensing of glucose based on SFS measurements. The resonance Rayleigh scattering was monitored by measuring synchronous fluorescence spectroscopy at $\Delta\lambda = 0$ nm. The sensitivity of the SFS signal increased with a decrease in the size of the AuNPs. Accordingly, modulation of the physical properties of the AuNPs may be used to alter the sensitivity of the SFS signal. Efforts are underway to modulate the physical properties of the AuNPs in order to increase the SFS response as a function of analyte concentration.

2. 3.2.1. non-enzymatic sensing of glucose by AuNPs in the presence and absence of nafion

Fig. 2.11a shows the SFS signal of functional trialkoxysilane-stabilized AuNPs in the absence and presence of various concentrations of glucose. Fig. 2.11b shows the SFS signal in the presence of glucose and the interferent ascorbic acid. This result shows the selectivity of the approach for non-enzymatic sensing of glucose. The micellar activity of the functional trialkoxysilane allows the incorporation of an ion exchanger such as nafion with the functional trialkoxysilane-stabilized gold nanoparticles. Fig. 2.11c and Fig. 2.11d show the results from

the nafion incorporated gold nanoparticles; these results indicate the dependence of the SFS signal on the glucose concentration. Also, the results show an enhancement in the SFS signal for glucose in the presence of nafion. Moreover, the SFS signal for ascorbic acid (5 mM) is significantly reduced. These results show the effectiveness of these AuNPs for enzyme-free sensing of glucose. The role of other metal nanoparticles and multimetallic nanoparticles for enzyme-free sensing of glucose was also assessed. Since AuNPs display excellent SFS activity for enzyme-free sensing of glucose (Fig. 2.11).
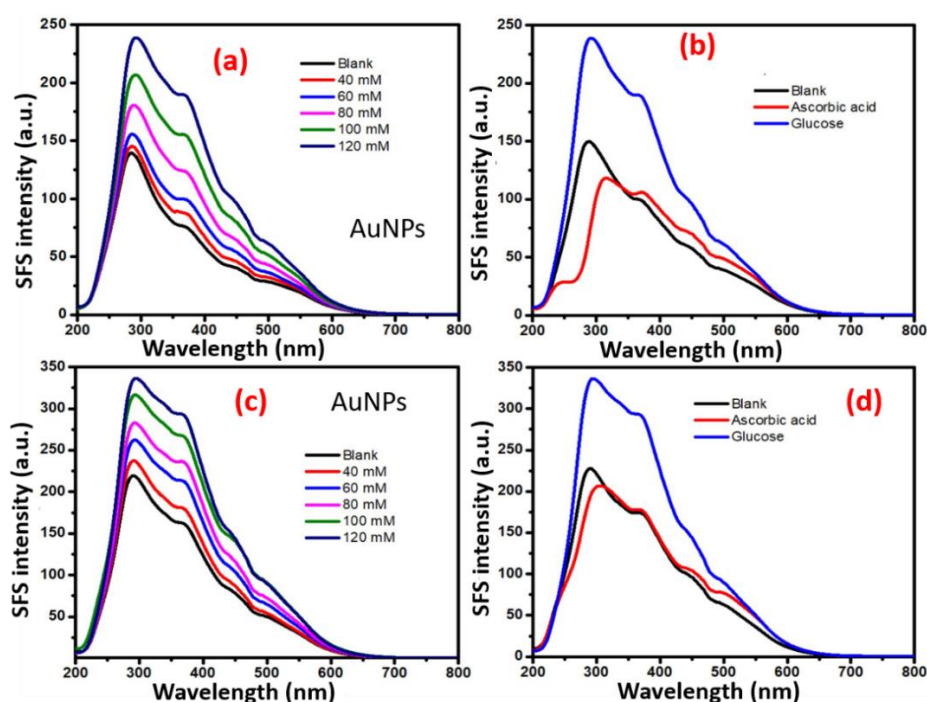

Fig. 2.11. (a) Synchronous fluorescence spectra at delta $\Delta\lambda = 0$ nm, the spectra were recorded at various concentrations of glucose. (b) Synchronous fluorescence intensity of AuNPs in the presence of glucose and ascorbic acid. (c) Synchronous fluorescence spectra at delta $\Delta\lambda = 0$ nm, the spectra were recorded at different concentrations of glucose with nafion. (d) Synchronous fluorescence intensity of AuNPs with nafion in the presence of glucose and ascorbic acid.

2. 3.2.2. Non-enzymatic sensing of glucose by using Au-Pd bimetallic nanoparticles with different metal ratio in the presence of nafion

We attempted to understand the role of bimetallic Au-Pd NPs made with different ratios of both metal cations. To understand the variation of the SFS signal with the composition of the bimetallic nanoparticles, Au-Pd bimetallic nanoparticles were made with 20:80 and 80:20 gold: palladium ratios
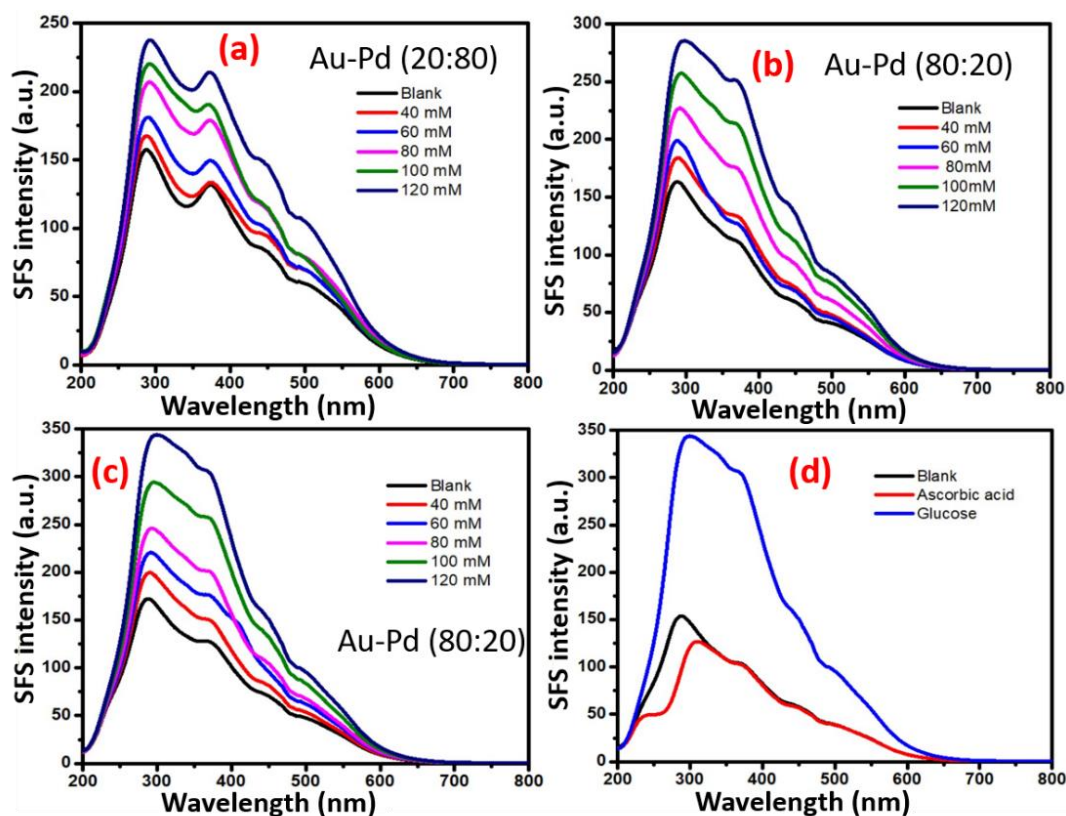

Fig. 2.12. Synchronous fluorescence spectra at delta $\Delta\lambda = 0$ nm; the spectra were recorded at various concentrations of glucose. (a) Synchronous fluorescence intensity of bimetallic (Au-Pd) NPs with an Au:Pd ratio of 20:80. (b) Synchronous fluorescence intensity of bimetallic (Au-Pd) NPs with an Au:Pd ratio of 80:20. (c) Synchronous fluorescence intensity of bimetallic (Au-Pd) NPs with an of ratio Au:Pd 80:20 with nafion. (d) Synchronous fluorescence intensity of bimetallic (Au-Pd) NPs with an Au:Pd ratio of 80:20 with nafion in the presence of glucose and ascorbic acid.

The results from the variation of the SFS signal as a function of glucose concentration with as-made bimetallic nanoparticles are shown in Fig. 2.12 the result from the as-made bimetallic nanoparticles with a 20:80 Au:Pd ratio is shown in Fig. 2.12a and the result of nanoparticles with the same made at an 80:20 Au:Pd ratio is shown in Fig. 2.12b. These results confirm that an increase in the palladium content results in a decrease in the SFS signal; the bimetallic NPs made with an 80:20 Au:Pd ratio show better sensitivity than those made at a 20:80 ratio of Au:Pd and also compared to that of only AuNPs (Fig. 2.11), this result indicates the utility of these bimetallic nanoparticles for glucose sensing. The incorporation of nafion with the bimetallic nanoparticles made with 80:20 of Au: Pd shows better sensitivity for glucose sensing (Fig. 2.12c) as compared to that in the absence of nafion (Fig. 2.12 b). The calibration curves for the analysis of glucose based on SFS intensity at $\Delta\lambda = 0$ nm, using AuNP at wavelength 369 nm are shown in Fig. 2.13a, similar results with Au-Pd bimetallic NPs made with an 80:20 ratio at a wavelength of 371 nm are shown in Fig. 2.13b. These results confirm that the bimetallic Au-Pd nanoparticles have high sensitivity for glucose analysis in the presence of Nafion and also justify the red shift for better enzyme free sensing of glucose. We also investigated the role of other monometallic, bimetallic and trimetallic nanoparticles (e.g., Ag NPs, Pd NPs, Ag-Au NPs, and Ag-Au-Pd NPs) to understand their SFS signal as a function of the glucose concentration.
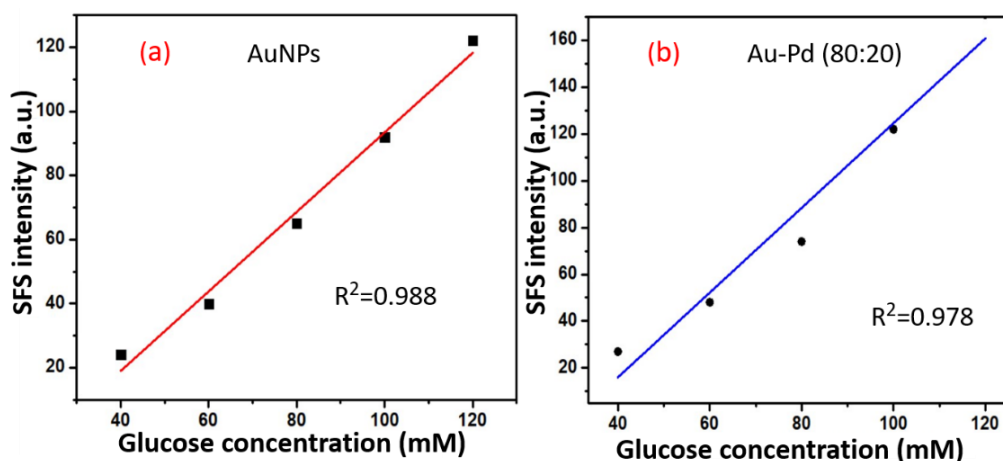
Fig. 2.13. Linear plot (a) Concentration of glucose versus synchronous fluorescence spectroscopy (SFS) intensity in the presence of AuNPs with Nafion. (b) The concentration of glucose versus SFS intensity in the presence of bimetallic Au-Pd nanoparticles with an Au:Pd ratio of 80:20 with nafion.

2. 3.2.3. Non-enzymatic sensing of glucose by using Ag and Pd monometallic nanoparticles

Non enzymatic sensing of glucose using AgNPs and PdNPs and the graph shows in Fig. 2.14 indicate the dependence of the SFS signal on the glucose concentration with AgNPs (Fig. 2.14a) and PdNPs (Fig. 2.14c), respectively. Also, the results in the presence of ascorbic acid have been shown in Fig. 2.14b and Fig. 2.14d, respectively. These results indicate that AgNPs are the least sensitive in terms of the SFS signal produced as a function of the glucose concentration, PdNPs were noted to show better sensitivity than AgNPs (Fig. 2.14). Furthermore, the presence of gold and silver as Ag-Au bimetallic NPs also significantly reduces the sensitivity of the SFS signal as a function of the glucose concentration (Fig. 2.15), this result suggests the presence of silver was associated with a decrease in SFS signal as a function of the glucose concentration.
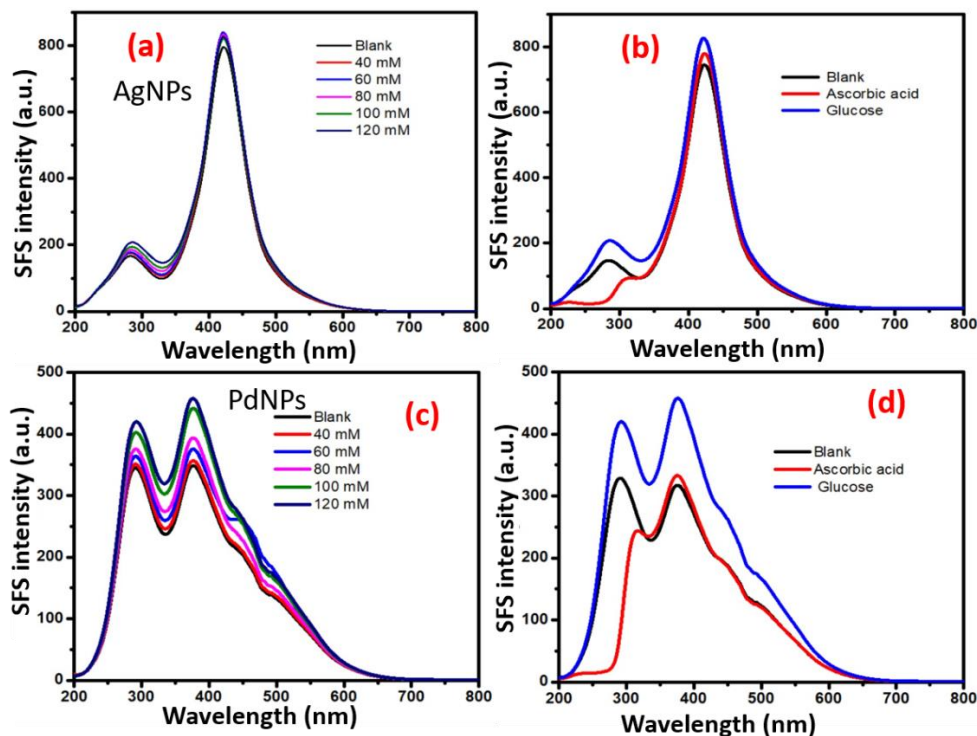
Fig. 2.14. Synchronous fluorescence spectra at delta $\Delta\lambda = 0$ nm, recorded at various concentrations of glucose. (a) AgNPs (b) Synchronous fluorescence intensity of AgNPs in the presence of glucose and ascorbic acid. (c) PdNPs. (d) Synchronous fluorescence intensity of PdNPs in the presence of glucose and ascorbic acid.

2. 3.2.4. Non-enzymatic sensing of glucose by using Ag-Pd, Au-Ag bimetallic and Au-Ag-Pd trimetallic nanoparticles

The variation of the SFS signal from Ag-Pd, Ag-Au, and Au-Ag-Pd NPs as a function of the glucose concentration is shown in Fig. 2.15. Fig. 2.15a, Fig. 2.15b and Fig. 2.15c indicate that the bimetallic and trimetallic NPs that contain Ag as one of constituents are not potentially active for non-enzymatic glucose sensing based on synchronous fluorescence spectroscopy (Fig. 2.15), this result confirm the finding related to the role AgNPs as recorded in Fig. 2.14a
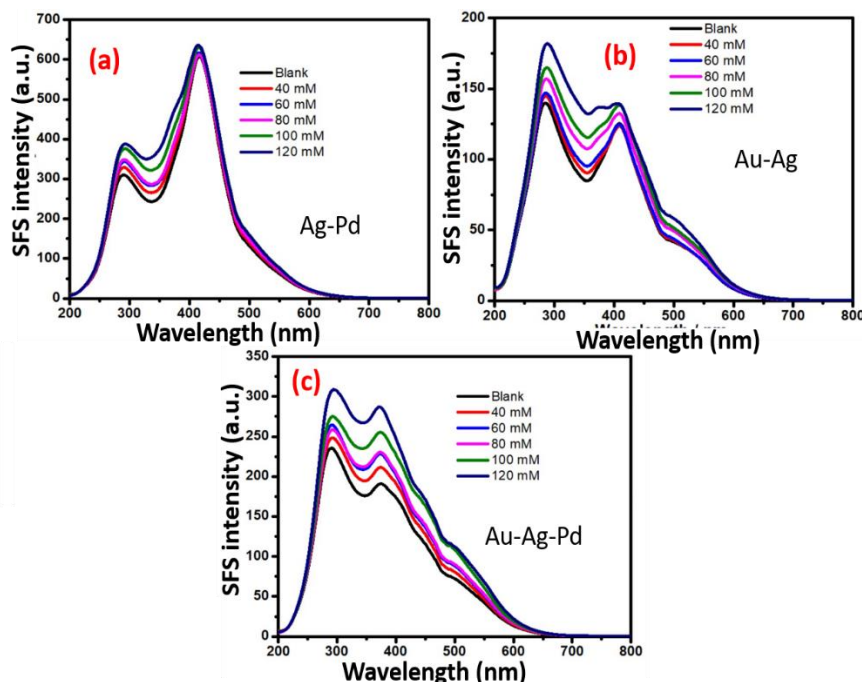
Fig. 2.15. Synchronous fluorescence spectra at $\Delta\lambda = 0$ nm recorded at various concentration of glucose: (a) bimetallic (Ag-Pd) NPs, (b) bimetallic (Ag-Au) NPs, and (c) trimetallic (Au-Ag-Pd) NPs.

2. 4. Conclusions

This study describes functional trialkoxysilane-mediated synthesis of monometallic, bimetallic, and trimetallic noble metal nanoparticles with high stability for potential use in enzyme free detection of glucose based on synchronous fluorescence spectroscopy (SFS). The impact of the monometallic, bimetallic, and trimetallic noble metal nanoparticles, (AuNPs, AgNPs, PdNPs, Ag-Au NPs, Au-Pd NPs, Ag-Pd NPs, and Au-Ag-Pd NPs) on the variation of the SFS signal for non-enzymatic sensing of glucose was demonstrated. The finding predicts that bimetallic Au-Pd NPs made with an 80:20 Au:Pd ratio display excellent results for glucose sensing. The micellar activity of the as-made nanomaterials can be effectively explored for making nafion-metal nanoparticles colloidal suspensions for non-enzymatic detection of glucose.